Available online at www.sciencedirect.com
ScienceDirect
Scripta Materialia 63 (2010) 1136–1139
Scripta MATERIALIA
www.elsevier.com/locate/scriptamat

# Nanoindentation and plasticity in nanocrystalline Ni nanowires: A case study in size effect mitigation

Frederic Sansoz[a,*] and Virginie Dupont[b]

[a] School of Engineering and Materials Science Program, University of Vermont, Burlington, VT 05405, USA
[b] Theoretical Division, Los Alamos National Laboratory, P.O. Box 1663, MS B268, Los Alamos, NM 87545, USA

Received 19 June 2010; revised 9 August 2010; accepted 12 August 2010
Available online 17 August 2010

We examine the processes of spherical indentation and tension in Ni nanowires and thin films containing random distributions of nanoscale grains by molecular dynamics simulations. It is shown that the resistance to nanoindentation of nanocrystalline Ni nanowires with diameters of 12 and 30 nm tends not to depend on the wire diameter and free surfaces, contrary to nanoindentation in single-crystalline nanowires. Accommodation of plastic deformation by grain boundary sliding suggests a mitigation strategy for sample boundary effects in nanoscale plasticity.


*Keywords:* Nanowire; Nanocrystalline microstructure; Nanoindentation; Plasticity

The mechanical behavior of metallic nanowires (NWs) and micropillars (MPs) is found to exhibit a pronounced dependence on sample size, which does not exist with macroscopic properties in bulk metals [1–9]. In particular, pure tension and compression experiments in single-crystalline NWs and MPs made of face-centered cubic (fcc) metals, such as Ni and Au, have shown evidence for a drastic increase in plastic flow stress with a size reduction in the sub-micron regime; a phenomenon proving that "smaller is stronger" under tension or compression [1–7]. On the contrary, nanoindentation studies in single-crystal fcc MPs and NWs [10–13] have revealed a decrease in Young's modulus and hardness as the specimen size decreases; thus leading to an inverse scaling behavior where smaller NWs appear less resistant to contact loads than thicker ones. Therefore, the loading modes resulting from different characterization techniques strongly influence the study of size effects on strength and plasticity in NWs. The softening behavior observed during nanoindentation of single-crystal NWs can be interpreted by sample boundary effects on crystal plasticity, where the interaction of lattice dislocations emitted beneath the contacting tip, and their easy absorption by free surfaces, become more frequent and predominant as the sample diameter decreases [12]. Since metallic NWs are basic building blocks at the nanoscale level in electronic and electromechanical devices, it is critically important to alleviate such inverse size effects on plastic flow in fcc metal NWs when subjected to nanoindentation.

In this paper, we report on a possible mitigation strategy for sample boundary effects in metallic NWs under nanoindentation when NWs are nanostructured with a random distribution of nanoscale grains smaller than the wire diameter. Molecular dynamics (MD) simulations are used to gain fundamental insight into the processes of nanoindentation and pure tension in nanocrystalline Ni NWs with a mean grain size of 7 nm. This type of metallic NW is representative of realistic fcc metal NWs that can readily be produced with polycrystalline microstructures during synthesis [14,15]. Simulations in thin Ni films with identical grain size were also performed to study the intrinsic effect of free surfaces in the indentation of nanocrystalline Ni NWs. Here, we show a phenomenon of size invariance in the resistance to nanoindentation of nanocrystalline Ni NWs, in stark contrast to nanoindentation in single-crystalline NWs. The mechanisms of plasticity in deformed nanocrystalline Ni NWs are analyzed at atomic level by using least-squares atomic local shear strain invariant calculations [16] in order to explain this effect.

Simulations of deformation in NWs and thin films by nanoindentation with a frictionless, spherical tip, as well as by pure tensile loading, were performed by MD with an embedded-atom method (EAM) following the methodologies described in earlier work by Sansoz and co-

* Corresponding author. Tel.: +1 802 656 3837; e-mail: frederic.sansoz@uvm.edu

1359-6462/$ - see front matter © 2010 Acta Materialia Inc. Published by Elsevier Ltd. All rights reserved.
doi:10.1016/j.scriptamat.2010.08.028

workers [12,17]. In this study, we used an EAM interatomic potential for Ni from Mishin et al. [18]. The NWs were 40 nm in length, with diameters of 12 and 30 nm as shown in the inset of Figure 1. Periodic boundary conditions were applied along the wire axis to model an infinitely long NW. To simulate thin films, the whole simulation box (40 × 40 nm) was filled with atoms and periodic boundary conditions were applied to the directions parallel to the film surface. The film thicknesses were equal to the two NW diameters studied, i.e. 12 and 30 nm. Both thin film and NW models were constructed with a random distribution of grains with a mean size of 7 nm using a 3D Voronoi tessellation technique and an arbitrary crystal orientation [19]. The number of atoms ranged from ~0.4 million (12 nm diameter NW) to 4.4 million (30 nm thick film). The simulations presented in this work required ~25,000 computer processing unit (CPU) hours. Prior to deformation, all models were relaxed in two steps. First, we performed an energy minimization with a conjugate gradient method. Second, a zero stress relaxation in the isothermal–isobaric ensemble (constant number of particles, pressure and temperature, NPT) using a Nosé–Hoover thermostat was performed at 300 K for 125 ps (25,000 steps). The time step was 5 fs. Deformation was subsequently carried out at the same temperature in the canonical ensemble (constant number of particles, volume and temperature, NVT). To simulate the process of nanoindentation, the bottom two atomic layers were fixed in all directions to enable tip penetration into the specimens, while preventing rolling or sliding during deformation. The tip was modeled as a virtual sphere of 18 nm in diameter by a repulsive force with a force constant equal to 10 N m$^{-2}$ [12,20–22]. A gap of 0.2 nm was initially imposed between the sample surface and the tip. The tip was displaced at a rate of 1 m s$^{-1}$. The final depth of indentation into the samples was 1.8 nm (400,000 steps). The atomic positions were recorded at 10 ps intervals (2000 steps). The contact zone was defined by the atoms positioned within the boundary of the virtual indenter. The mean contact pressure was calculated by dividing the total force on the indenter by the projected area of contact determined directly from the contacted atom positions. To simulate pure tensile deformation, the NWs were deformed by straining the simulation box along the wire axis at a constant engineering strain rate of $5 \times 10^7$ s$^{-1}$. The mechanisms of plastic deformation were analyzed quantitatively by calculating the least-squares atomic local shear strain invariant [16] in the atomistic configuration viewer AtomEye [23]. In this paper, atoms in dark color are atoms undergoing negligible plastic deformation, while atoms in severely deformed zones with more than 30% plastic deformation appear in white color. As shown below, this visualization technique enables accurate detection of both intergranular and intragranular modes of plastic deformation in nanocrystalline solids.

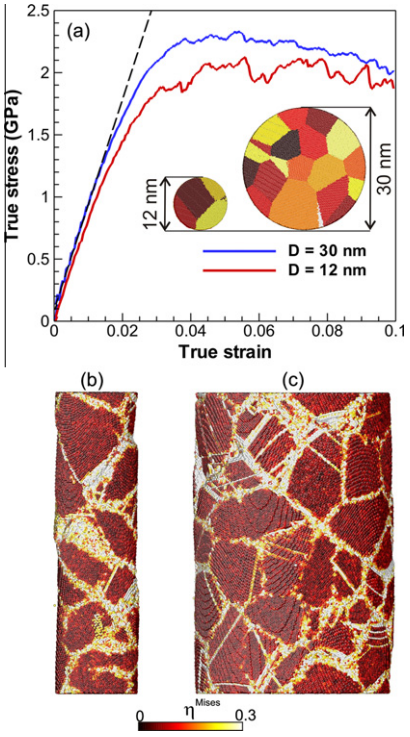


**Figure 1.** Molecular dynamics simulation of plasticity in nanocrystalline Ni nanowires under pure tension. (a) True stress–strain curves for 12 and 30 nm Ni nanowires with a mean grain size of 7 nm. Atomic-level snapshot at 10% deformation in Ni nanowires with a diameter equal to (b) 12 nm and (c) 30 nm. Coloring corresponds to the least-squares atomic local shear strain invariant ($\eta^{Mises}$), which shows that more plastic deformation is accommodated by grain boundary sliding than by the propagation of lattice dislocations.

The tensile behavior of the two nanocrystalline Ni NWs investigated is represented in Figure 1. For both NWs, the figure shows no sharp yielding point. Instead, the behavior becomes rapidly non-linear at an applied stress of ~1.3 GPa. This effect predominantly results from a localization of plastic deformation at grain boundaries, as shown in Figure 1b,c, where intense interface sliding is observed in all grain boundaries present in the models. The yield stress at 0.2% plastic strain is found equal to 1.45 and 1.69 GPa in the 12 and 30 nm NWs, and the maximum stress to 2.13 and 2.33 GPa, respectively. The lower overall flow stresses in the 12 nm NW as compared to the 30 nm NW in tension can be explained by the higher propensity to deform at grain boundaries due to free surface effects. Intergranular deformation is generally accompanied with serrated plastic flow [24], which is also more clearly evident in the stress–strain curve of the 12 nm diameter NW in Figure 1a, than in the curve for the 30 nm diameter NW. This result confirms earlier reports by Monk and Farkas [25,26] who have also used MD simulations to study the effect of diameter on the uniform deformation of nanocrystalline Ni NWs with mean grain sizes less than 10 nm. They found that the importance of dislocation-mediated plasticity decreases, while grain boundary sliding dramatically increases, in nanocrystalline NWs less than 36 nm in diameter and that such effect is more significant in tension than compression.

We now shift focus on the process of spherical indentation in NWs identical to those presented in Figure 1. Figure 2 shows different cross-sectional views of the 30 nm diameter NW deformed in its center by the virtual tip up to a penetration depth of 1.8 nm, which corresponds to a radial strain of 6% relative to the NW diameter. We observe in this case that the least-squares

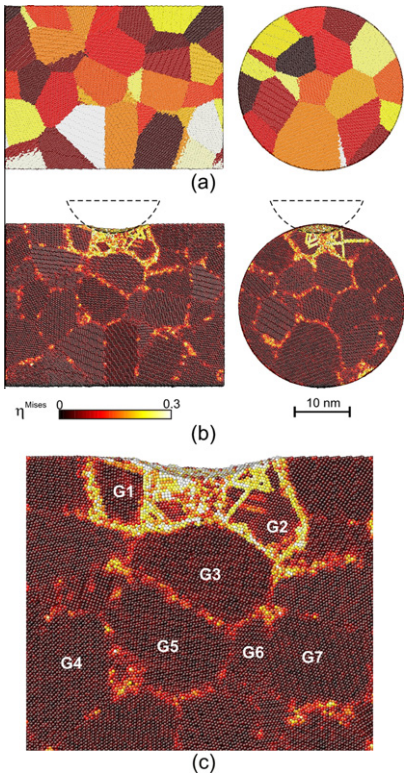


**Figure 2.** Atomic-level snapshot of deformation under spherical indentation in the 30 nm Ni nanowire presented in Figure 1. (a) Interior grain distribution prior to deformation. (b) After nanoindentation using a spherical tip of 18 nm in diameter. Coloring corresponds to the least-squares atomic local shear strain invariant ($\eta^{Mises}$). (c) Close-up view on the contact zone.

atomic local shear strain exceeds 30% within only a few grains in direct contact with the tip, such as grains G1 and G2 as shown in Figure 2c, while no significant plastic deformation occurs in the adjacent grains, e.g. grains G3–G7. Figure 2b and c show that grain boundary sliding is predominant; similar to the mechanism under pure tension, but for penetration depths larger than 1 nm we also find more dislocation emissions from grain boundaries. The latter is indicative of the elimination of free volume and defects within grain boundaries by atomic shuffling, which has also been observed in the sliding of symmetric tilt grain boundaries in bicrystals subjected to pure shear deformation [27]. This could suggest that grain boundary sliding in Ni NWs is more severe in nanoindentation than in pure tension. Furthermore, the same mechanism was found to operate in 12 nm diameter NWs (not shown) and, in particular, to extend entirely through the cross-section of these NWs due to the size reduction.

The mechanical response under nanoindentation simulated in both thin films and NWs with identical grain sizes is presented in Figure 3. Most of the differences in the force–penetration curves shown in Figure 3a,c are due to geometric effects on the contact area between film and NW models, where such effects are found to be independent of the specimen microstructure, either single-crystalline or nanocrystalline, during nanoindentation of NWs [12,28]. However, Figure 3b,d reveals that there are no marked differences in terms of the mean contact

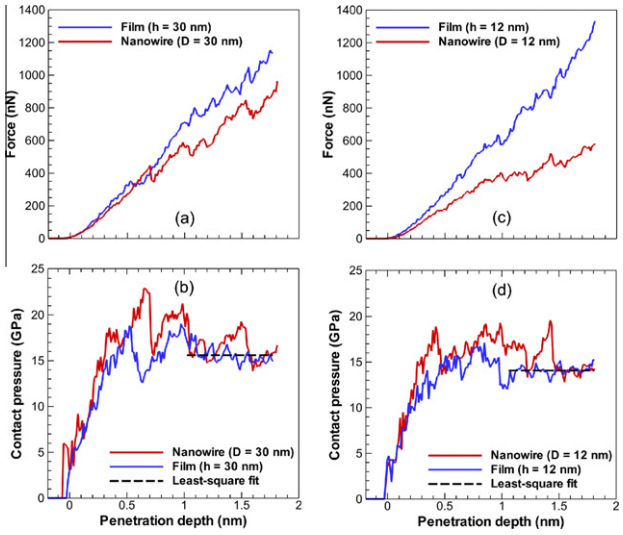


**Figure 3.** Simulated force–displacement and contact pressure nanoindentation curves in nanocrystalline Ni thin films and nanowires indented with a spherical tip of 18 nm in diameter. The mean grain size is 7 nm. $D$ and $h$ represent the nanowire diameter and film thickness, respectively.

pressure as a function of penetration depth between NW and thin film models, which shows no size effect as opposed to the NWs deformed in tension as shown in Figure 1a. To support this conclusion in a more quantitative manner, we present in Table 1 the mean contact pressure averaged over penetration depths $\geqslant 1$ nm, which corresponds in our simulations to a regime of constant pressures after the yield point, as shown by the least-squares fit in the film model in Figure 3b,d. For comparison, Table 1 also presents the values of mean contact pressures in single-crystalline Ni NWs obtained in an earlier work [12]. It is important to note that data presented in Table 1 for both single-crystalline and nanocrystalline models have been obtained by strictly using the same loading conditions including the same tip velocity and strain rate. This table shows that the resistance to nanoindentation in single-crystalline Ni is noticeably smaller in NWs than in thin films. This result is due to boundary effects on the easy annihilation of dislocations at free surfaces [12], which are more significant and result in lower contact pressures when the NW diameter is 12 nm. In contrast, the present study demonstrates that the resistance to nanoindentation in nanocrystalline Ni is somewhat larger in NWs than in thin films. For exam-

**Table 1.** Plasticity size effects in nanoindentation of nanowires and thin films with either single-crystalline or nanocrystalline structures simulated by MD method. The mean grain size in the nanocrystalline models is 7 nm. The mean contact pressure is obtained by averaging the contact pressures over penetration depths larger than 1 nm.

| Structure | Diameter/thickness (nm) | Mean contact pressure (GPa) | |
|---|---|---|---|
| | | Nanowire | Thin film |
| Single-crystalline [12] | 30 | 18.0 | 19.9 |
| | 12 | 13.8 | 21.4 |
| Nanocrystalline | 30 | $16.5 \pm 1.4$ | $15.8 \pm 1.1$ |
| | 12 | $15.4 \pm 1.6$ | $14.0 \pm 0.7$ |

ple, the mean contact pressure is found equal to $15.4 \pm 1.6$ and $14.0 \pm 0.7$ GPa, respectively, for a NW/film size of 12 nm. Furthermore, the change in mean contact pressure from one NW size to another is within the measured standard deviation, and therefore can be considered as negligible. This major finding therefore suggests that plastic deformation in nanocrystalline Ni NWs under nanoindentation is governed by the grain size rather than the NW diameter, and is predominantly accommodated by grain boundary sliding rather than the propagation of lattice dislocations.

In macroscopic samples, size effects on indentation are influenced primarily by two factors: (1) strain-gradient plasticity effects [29] and (2) the relevant microstructure length scale such as the mean grain size, which is often comparable to or smaller than the tip radius. As grain size decreases, a transition in deformation mechanism during nanoindentation is found to take place from intragranular lattice activities involving full dislocations, extended partial dislocations and mechanical twins to grain boundary-mediated deformation processes involving interface sliding and grain rotation [19–22,24].

In contrast, size effects on plasticity in nanoscale structures such as Ni NWs emerge because the material strength predominantly depends on the deformation length such as diameter and volume, as opposed to the microstructure length scale. For NWs less than 30 nm in diameter, dislocations can easily escape at free boundaries because strain-gradient plasticity no longer applies for very shallow depths of indentations [30], which cause important softening effects in smaller NWs during indentation [10–13]. However, the present atomistic simulations point to the conclusion that microstructure plays a key role in governing the plasticity and fracture properties of metals at the nanoscale, and their size dependence. In particular, we demonstrate here that it is still possible to produce realistic polycrystalline microstructures in Ni NWs in order to eliminate softening effects during indentation, which are detrimental for mechanical properties at the nanoscale.

In summary, we can conclude from the MD simulations presented in this work that the resistance to nanoindentation in Ni NWs containing a random distribution of nanoscale grains is size-invariant, and that sample boundary effects that commonly lead to significant softening in single-crystalline fcc NWs and MPs subjected to nanoindentation, are strongly decreased, if not eliminated, by nanostructuring. This behavior was shown to result from the mechanisms of grain boundary sliding and grain boundary-mediated dislocation emission, which make the material strength depend predominantly on the grain size, rather than the NW diameter. This finding is relevant for designing more robust nanoscale devices based on metallic NWs for engineering applications. For reproducibility, it would also be necessary to confirm that the hardness (or contact pressure) does not depend on the crystallographic orientations of the nanograins and the mismatch angles at grain boundaries, which requires more hardness measurements in both nanocrystalline films and NWs using a combination of experimental and simulation approaches.

Support from NSF CAREER program (grant DMR-0747658) and the computational resources provided by the Vermont Advanced Computing Center (NASA grant NNX06AC88G) are gratefully acknowledged. The simulations shown in this work were performed using LAMMPS [31].

[1] M.D. Uchic, D.M. Dimiduk, J.N. Florando, W.D. Nix, Science 305 (2004) 986.
[2] D.M. Dimiduk, M.D. Uchic, T.A. Parthasarathy, Acta Mater. 53 (2005) 4065.
[3] B. Wu, A. Heidelberg, J.J. Boland, Nat. Mater. 4 (2005) 525.
[4] J.R. Greer, W.D. Nix, Phys. Rev. B 73 (2006) 245410.
[5] C.A. Volkert, E.T. Lilleodden, Phil. Mag. 86 (2006) 5567.
[6] Z.W. Shan, R.K. Mishra, S.A. Syed Asif, O.L. Warren, A.M. Minor, Nat. Mater. 7 (2008) 115.
[7] R. Dou, B. Derby, Scripta Mater. 59 (2008) 151.
[8] D. Kiener, W. Grosinger, G. Dehm, R. Pippan, Acta Mater. 56 (2008) 580.
[9] G. Richter, K. Hillerich, D.S. Gianola, R. Monig, O. Kraft, C.A. Volkert, Nano Lett. 9 (2009) 3048.
[10] Y. Choi, S. Suresh, Scripta Mater. 48 (2003) 249.
[11] X. Li, H. Gao, C.J. Murphy, K.K. Caswell, Nano Lett. 3 (2003) 1495.
[12] V. Dupont, F. Sansoz, J. Mater. Res. 24 (2009) 948.
[13] J. Lian, J.-Y. Kim, J.R. Greer, J. Wang, J. Mech. Phys. Solids 57 (2009) 812.
[14] A.J. Yin, J. Li, W. Jian, A.J. Bennett, J.M. Xu, Appl. Phys. Lett. 79 (2001) 1039.
[15] M. Tian, J. Wang, J. Kurtz, T.E. Mallouk, M.H.W. Chan, Nano Lett. 3 (2003) 919.
[16] F. Shimizu, S. Ogata, J. Li, Mater. Trans. 48 (2007) 2923.
[17] C. Deng, F. Sansoz, Nano Lett. 9 (2009) 1517.
[18] Y. Mishin, D. Farkas, M.J. Mehl, D.A. Papaconstantopoulos, Phys. Rev. B 59 (1999) 3393.
[19] V. Dupont, F. Sansoz, Multiscale modeling of contact-induced plasticity in nanocrystalline metals, in: T. Dumitrica (Ed.), Trends in Computational Nanomechanics, Series: Challenges and Advances in Computational Chemistry and Physics, vol. 9, Springer, Netherlands, 2010, pp. 151–172.
[20] E.T. Lilleodden, J.A. Zimmerman, S.M. Foiles, W.D. Nix, J. Mech. Phys. of Solids 51 (2003) 901.
[21] D. Feichtinger, P.M. Derlet, H. Van Swygenhoven, Phys. Rev. B 67 (2003) 024113.
[22] A.K. Nair, E. Parker, P. Gaudreau, D. Farkas, R.D. Kriz, Int. J. Plasticity 24 (2008) 2016.
[23] J. Li, Modelling Simul. Mater Sci. Eng. 11 (2003) 173.
[24] F. Sansoz, V. Dupont, Mater. Sci. Eng., C 27 (2007) 1509.
[25] J. Monk, D. Farkas, Phys. Rev. B 75 (2007) 045414.
[26] J. Monk, D. Farkas, Phil. Mag. 87 (2007) 2233.
[27] F. Sansoz, J.F. Molinari, Acta Mater. 53 (2005) 1931.
[28] G. Feng, W.D. Nix, Y. Yoon, C.J. Lee, J. Appl. Phys. 99 (2006) 074304.
[29] W.D. Nix, H. Gao, J. Mech. Phys. Solids 46 (1998) 411.
[30] W.W. Gerberich, N.I. Tymiak, J.C. Grunlan, M.F. Horstemeyer, M.I. Baskes, J. Appl. Mech. 4 (2002) 433.
[31] S.J. Plimpton, J. Comp. Phys. 117 (1995) 1.